Imaginary part of the optical conductivity of $Ba_{1-x}K_xBiO_3$

F. Marsiglio
Neutron and Condensed Matter Science, Atomic Energy of Canada Limited, Chalk River Laboratories, Chalk River, Ontario, Canada KOJ 1JO;
Department of Physics and Astronomy, McMaster University, Hamilton, Ontario, Canada L8S 4M1;
and Canadian Institute for Advanced Research, McMaster University, Hamilton, Ontario, Canada L8S 4M1

J. P. Carbotte
Department of Physics and Astronomy, McMaster University, Hamilton, Ontario, Canada L8S 4M1
and Canadian Institute for Advanced Research, McMaster University, Hamilton, Ontario, Canada L8S 4M1

A. Puchkov
Department of Physics and Astronomy, McMaster University, Hamilton, Ontario, Canada L8S 4M1

T. Timusk
Department of Physics and Astronomy, McMaster University, Hamilton, Ontario, Canada L8S 4M1
and Canadian Institute for Advanced Research, McMaster University, Hamilton, Ontario, Canada L8S 4M1
(Received 28 August 1995)

The frequency dependence of the imaginary part of the infrared conductivity is calculated for a superconductor. Sharp structure, characteristic of superconductivity with an order parameter with *s*-wave symmetry, appears in the BCS limit as a minimum at a frequency equal to twice the gap value. This structure scales with temperature but gets progressively smeared and shifted as impurity scattering is increased. The relationship between low-frequency results and the zero-frequency limit is investigated. Experimental results on $Ba_{1-x}K_xBiO_3$ are also presented. The low-frequency imaginary part of the conductivity displays a minimum at $2\Delta \approx 12$ meV, and provides unequivocal evidence of an *s*-wave superconducting order parameter. Strong-coupling (Eliashberg) results show similar trends. Using this formulation we find that the electron-phonon coupling in $Ba_{1-x}K_xBiO_3$ must necessarily be small, with coupling constant $\lambda \approx 0.2$, in agreement with conclusions drawn from measurements of the real part of the conductivity. Thus $Ba_{1-x}K_xBiO_3$ is an *s*-wave superconductor that is not driven by the conventional electron-phonon interaction.

I. INTRODUCTION

Optical conductivity data in the infrared can give important information on the properties of the low-energy excitations present, and, in particular, on the scattering rate.[1] In Drude theory, the width of the real part of the conductivity gives the inverse of the scattering time, which can be a combination of elastic impurity scattering and inelastic (e.g., phonon-mediated) scattering. In the latter case, a process, phonon-assisted absorption, becomes possible.[2] This process does not exist with impurity scattering alone, and makes an additional contribution to both the real and imaginary parts of the conductivity.

In the past most discussions of the infrared conductivity in an electron-phonon system have concentrated on the real part of the conductivity.[1] Very few results are available on the imaginary part which nonetheless follows uniquely from the real part through a Kramers-Kronig relation. Recently experimentalists have effectively exploited the relationship between the inverse square of the penetration depth and the zero-frequency limit of the imaginary part of the conductivity ($\lim_{\nu\to 0}\nu\sigma_2(\nu)=(c^2/4\pi)[1/\lambda^2(T)]$, where we use the convention that $\sigma=\sigma_1-i\sigma_2$, and λ here is the penetration depth), to obtain information on this important quantity from the far-infrared optical conductivity.[3]

The purpose of this paper is to study the frequency dependence of $\nu\sigma_2(\nu)$. We start with the BCS model[4] and then generalize to an Eliashberg strong-coupling system. The aim is to understand how the more complicated effects due to the interactions with phonons modify the BCS results. The necessary theory is summarized in Sec. II. Results of BCS theory are presented in Sec. III. It is found that in an *s*-wave superconductor there will be a distinct minimum in $\nu\sigma_2(\nu)$ at twice the gap value. With the addition of impurities the minimum broadens and shifts slightly. The temperature dependence of the minimum tracks the gap temperature dependence. We also study how finite frequency results are related to the zero-frequency limit. Results are presented in Sec. IV for the strong-coupling case. The most significant difference between the Eliashberg and BCS approaches occurs in the pure case. In this limit, BCS theory no longer contains any scattering mechanisms, whereas inelastic scattering remains in an Eliashberg formalism, and we can study the effect of this additional source of scattering. In Sec. V, the specific case of $Ba_{1-x}K_xBiO_3$ (with $x=0.4$) will be considered. Comparison with infrared data will lead us to conclude that this system contains an isotropic *s*-wave order parameter, but is *not* an electron-phonon superconductor. The inelastic scattering observed in the conductivity at room temperature is inconsistent with a mass enhancement parameter of order

unity, which is required for an electron-phonon superconductor with $T_c \approx 30$ K. A summary is provided in Sec. VI.

II. FORMALISM

Expressions for the optical conductivity of an electron-phonon superconductor, excluding vertex corrections for the electron-phonon interactions, are now well established[5–13] and require solutions of the Eliashberg equations[14] for the pairing function $\phi(\omega)$ and renormalized frequency $\tilde{\omega}(\omega)$. For an isotropic s-wave electron-phonon superconductor, these equations take the form[15]

$$\phi(\omega)=\pi T\sum_{m=-\infty}^{\infty}[\lambda(\omega-i\omega_m)-\mu^*(\omega_c)\theta(\omega_c-|\omega_m|)]\frac{\phi_m}{\sqrt{\tilde{\omega}^2(i\omega_m)+\phi_m^2}}+i\pi\int_0^\infty d\nu\ \alpha^2F(\nu)$$
$$\times\left\{[N(\nu)+f(\nu-\omega)]\frac{\phi(\omega-\nu)}{\sqrt{\tilde{\omega}^2(\omega-\nu)-\phi^2(\omega-\nu)}}+[N(\nu)+f(\nu+\omega)]\frac{\phi(\omega+\nu)}{\sqrt{\tilde{\omega}^2(\omega+\nu)-\phi^2(\omega+\nu)}}\right\} \quad (1)$$

and

$$\tilde{\omega}(\omega)=1+i\pi T\sum_{m=-\infty}^{\infty}\lambda(\omega-i\omega_m)\frac{\tilde{\omega}(i\omega_m)}{\sqrt{\tilde{\omega}^2(i\omega_m)+\phi_m^2}}+i\pi\int_0^\infty d\nu\ \alpha^2F(\nu)\left\{[N(\nu)+f(\nu-\omega)]\frac{\tilde{\omega}(\omega-\nu)}{\sqrt{\tilde{\omega}^2(\omega-\nu)-\phi^2(\omega-\nu)}}\right.$$
$$\left.+[N(\nu)+f(\nu+\omega)]\frac{\tilde{\omega}(\omega+\nu)}{\sqrt{\tilde{\omega}^2(\omega+\nu)-\phi^2(\omega+\nu)}}\right\}. \quad (2)$$

In these equations $N(\nu)$ and $f(\nu)$ are the Bose and Fermi distribution functions, respectively, and $\lambda(z)$ is the Hilbert transform of the electron-phonon spectral function $\alpha^2F(\nu)$. $\mu^*(\omega_c)$ is the Coulomb repulsion parameter with cutoff ω_c. A negative value for this parameter can be used to model some BCS attraction of unspecified origin. The required functions are first obtained on the imaginary axis at the Matsubara frequencies, i.e., $\omega=i\omega_n\equiv i\pi T(2n-1)$, with $\phi_m\equiv\phi(i\omega_m)$ by setting the complex variable ω in these equations to the Matsubara frequencies.[16,17] Then the equations are iterated as written, with ω set to a frequency on the real axis.

From the numerical solutions of Eqs. (1) and (2), the conductivity follows from the paramagnetic response kernel, $\Pi(\nu+i\delta)$, given by[5,6,8–13]

$$\Pi(\nu+i\delta)=\frac{ne^2}{m}\left\{-1+\int_0^\infty d\omega\ \tanh\left(\frac{\beta\omega}{2}\right)[h_1(\omega,\omega+\nu)-h_2(\omega,\omega+\nu)]+\int_{-\nu}^{D}d\omega\ \tanh\left(\frac{\beta(\omega+\nu)}{2}\right)\right.$$
$$\left.\times[h_1^*(\omega,\omega+\nu)+h_2(\omega,\omega+\nu)]\right\} \quad (3)$$

with the conductivity

$$\sigma(\nu)=\frac{i}{\nu}\left(\Pi(\nu+i\delta)+\frac{ne^2}{m}\right), \quad (4)$$

where e is the magnitude of the charge on the electron, m its mass and n the number of electrons per unit volume. The functions h_i in Eq. (3) are given by

$$h_1(\omega_1,\omega_2)=\frac{1-N(\omega_1)N(\omega_2)-P(\omega_1)P(\omega_2)}{2[\epsilon(\omega_1)+\epsilon(\omega_2)]},$$

$$h_2(\omega_1,\omega_2)=\frac{1+N^*(\omega_1)N(\omega_2)+P^*(\omega_1)P(\omega_2)}{2[\epsilon(\omega_2)-\epsilon^*(\omega_1)]},$$

$$N(\omega)=\frac{\tilde{\omega}(\omega+i\delta)}{\epsilon(\omega+i\delta)},$$

$$P(\omega)=\frac{\phi(\omega+i\delta)}{\epsilon(\omega+i\delta)},$$

$$\epsilon(\omega)=\sqrt{\tilde{\omega}^2(\omega+i\delta)-\phi^2(\omega+i\delta)}. \quad (5)$$

The equations so far have been written for a clean system. To include normal impurity scattering in the Born approximation, an average scattering rate, $1/\tau$, is used, and gives rise to an additional contribution to the pairing and renormalization functions:

$$\phi(\omega)\rightarrow\phi(\omega)+\frac{i}{2\tau}\frac{\phi(\omega)}{\sqrt{\tilde{\omega}^2(\omega)-\phi^2(\omega)}}, \quad (6)$$

$$\tilde{\omega}(\omega)\rightarrow\tilde{\omega}(\omega)+\frac{i}{2\tau}\frac{\tilde{\omega}(\omega)}{\sqrt{\tilde{\omega}^2(\omega)-\phi^2(\omega)}}. \quad (7)$$

Equation (3) remains the same with impurity scattering. The modifications are all implicitly contained in the pairing and renormalization functions. Note that the gap parameter, $\Delta(\omega)\equiv\phi(\omega)/Z(\omega)$, remains the same, independent of the impurity scattering rate.

III. THE BCS LIMIT

The equations for the conductivity and pairing function discussed so far reduce in the BCS limit, thus simplifying the numerical work.[18–20] The result is a universal function for the conductivity, dependent only on the impurity scattering rate. In the BCS limit $\tilde{\omega}(\omega)$ is given by the bare frequency ω [plus the impurity scattering term given in Eq. (7)], and the pairing function $\phi(\omega)$ reduces to the BCS gap parameter, Δ [plus Eq. (6)]. The temperature dependence of $\Delta(T)$ is given by solution of the BCS equation. As already mentioned, the clean limit is pathological within BCS theory. To allow some scattering mechanism to remain some nonzero impurity scattering is required. Note that in the remainder of this paper we present results for the conductivity normalized to ne^2/m, so the only parameter in the BCS limit is the impurity scattering rate, $1/\tau$.

Results are shown in Fig. 1 for $\nu\sigma_2(\nu)$ as a function of frequency for a BCS model with $T_c=29$ K ($Ba_{1-x}K_xBiO_3$). We use (a) $1/\tau=1$, (b) $1/\tau=5$, and (c) $1/\tau=25$ meV, with differently styled curves for various temperatures, as explained in the figure caption. The largest scattering rate we have used is representative of the $Ba_{1-x}K_xBiO_3$ compounds, as we will see later.

For small scattering rate [Fig. 1(a)] the quantity $\nu\sigma_2(\nu)$ displays a cusplike minimum at a frequency equal to two times the temperature-dependent gap parameter. As the temperature increases towards T_c the size of the minimum decreases, and of course its location tracks the energy gap. For $1/\tau=1$ meV the cusplike minimum occurs at perhaps too low a frequency for temperatures near T_c to be observed with optical infrared techniques, but at least, in principle, this minimum can be used to measure the gap temperature dependence. Note that the cusp in the imaginary part of the conductivity simply reflects the sharp onset in the real part of the conductivity which occurs at $2\Delta(T)$. For larger impurity scattering rates the minimum broadens somewhat.

Another important feature of our results is the limit as the frequency goes to zero, which as stated earlier, gives the London penetration depth. We have verified that our low-frequency conductivity results extrapolate to the correct penetration depth, as computed from an imaginary axis formulation:[5,21]

$$\frac{c^2}{4\pi}\frac{1}{\lambda^2(T)}=\frac{ne^2}{m}\,\pi T\sum_{n=-\infty}^{\infty}\frac{\phi^2(i\omega_n)}{[\tilde{\omega}^2(i\omega_n)+\phi^2(i\omega_n)]^{3/2}}. \tag{8}$$

As is apparent from the figures, particularly for low scattering rate, this limit can only be probed with very low photon energy, certainly too low for the usual infrared range in conventional electron-phonon superconductors.

As the impurity scattering rate increases the low-frequency conductivity $\nu\sigma_2(\nu)$ deviates significantly from unity. This is expected since the penetration depth increases with impurity scattering in a BCS model. The effect is very pronounced in Fig. 1(c) where it is also seen that the minimum due to the gap is considerably broadened due to the impurity scattering. To see the effect of impurity scattering on the low-frequency conductivity more clearly we show in Fig. 2 results for various impurity scattering rates. All curves are calculated in the BCS limit and for reduced temperature,

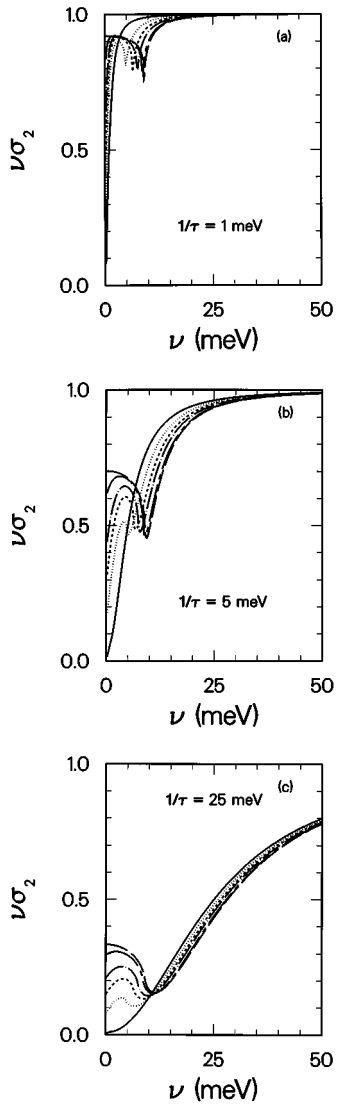

FIG. 1. The quantity $\nu\sigma_2(\nu)$ (imaginary part of the conductivity times the frequency in units of ne^2/m) vs frequency for various impurity scattering rates, (a) $1/\tau=1$, (b) $1/\tau=5$, and (c) $1/\tau=25$ meV. These results are calculated in the BCS limit with $T_c=29$ K. The zero-temperature gap value is given by $2\Delta_0/k_BT_c=3.53$ ($\Delta_0=8.8$ meV). The various curves correspond to different temperatures: $T/T_c=0.1$ (long-dashed), $T/T_c=0.5$ (long-dashed-short-dashed), $T/T_c=0.7$ (long-dashed-dotted), $T/T_c=0.8$ (short-dashed), $T/T_c=0.9$ (dotted), and $T/T_c=0.995$ (solid).

$T/T_c=0.1$, which is essentially zero temperature. As the scattering rate increases, the cusplike minimum broadens into a shallow minimum. For very high scattering rates, it is evident that extracting a gap value would be very difficult. The actual minimum is displaced to higher frequencies, and is no longer located at twice the gap.

The results of Figs. (1) and (2) immediately suggest the following question: To what extent can finite frequency conductivity data be used to extract information about the zero-frequency penetration depth? We first address the question of temperature dependence. The dimensionless quantity $\nu\sigma_2(\nu)$ is plotted in Fig. 3 as a function of reduced temperature, for various frequencies, as given in the figure caption. Two impurity scattering rates are used, (a) $1/\tau=1$ meV to represent a

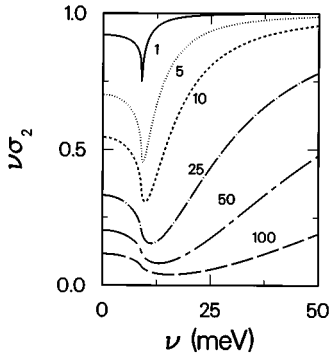

FIG. 2. $\nu\sigma_2(\nu)$ vs frequency for various impurity scattering rates. These results are in the BCS limit with $T/T_c=0.1$. The scattering rates are $1/\tau=1$ meV (solid), $1/\tau=5$ meV (dotted), $1/\tau=10$ meV (dashed), $1/\tau=25$ meV (dot-long-dashed), $1/\tau=50$ meV (short-dashed-long-dashed), and $1/\tau=100$ meV (long-dashed).

fairly clean case, and (b) $1/\tau=25$ meV, to represent both a dirtier case and $Ba_{1-x}K_xBiO_3$. In Fig. 3(a) the lowest-frequency curve plotted ($\nu=0.2$ meV) does indeed follow very closely the temperature dependence of the zero-frequency penetration depth. Nonetheless, already at $\nu=1.0$ meV (dotted curve) the temperature dependence of $\nu\sigma_2(\nu)$ deviates very markedly from that of the solid curve, and hence cannot be used to extract the temperature dependence of the penetration depth. As the impurity scattering increases the finite frequency results improve as is seen in Fig. 3(b).

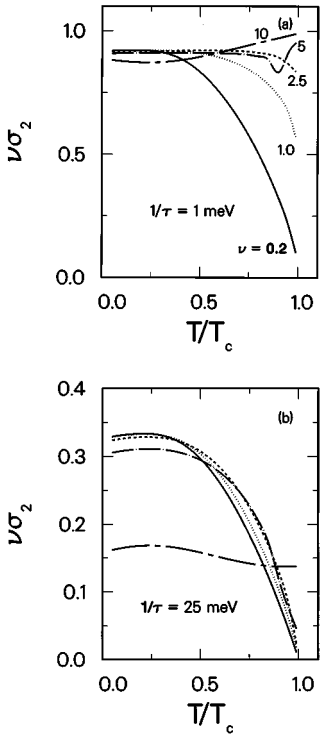

FIG. 3. $\nu\sigma_2(\nu)$ vs reduced temperature T/T_c in the BCS limit, plotted for various frequencies. The results are for (a) $1/\tau=1$ and (b) $1/\tau=25$ meV. The curves correspond to the frequencies $\nu=0.2$ meV (solid), $\nu=1.0$ meV (dotted), $\nu=2.5$ meV (dashed), $\nu=5.0$ meV (dot-dashed), and $\nu=10$ meV (short-dashed-long-dashed). The effect of finite frequency is more significant in the clean limit.

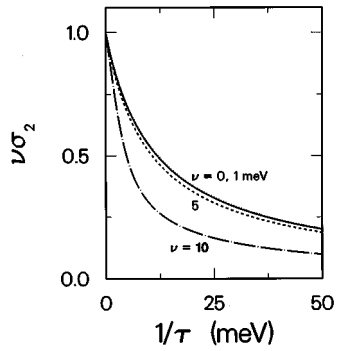

FIG. 4. $\nu\sigma_2(\nu)$ vs the impurity scattering rate $1/\tau$, for various frequencies. The results are in the BCS limit, with $T/T_c=0.1$. The curves correspond to $\nu=0$ (solid), 1 (dotted), 5 (dashed), and 10 meV (dot-dashed).

Clearly the finite frequency results give a good qualitative estimate of the temperature variation of the penetration depth up to $\nu=2.5$ meV. For frequencies of order twice the gap (e.g., $\nu=10$ meV), however, all correspondence with the penetration depth is lost.

Can finite frequency data be used to extract the impurity dependence of the penetration depth? In the BCS limit, with $\alpha\equiv 1/2\Delta\tau$,[22]

$$\frac{1}{\lambda^2(T=0)}=\frac{1}{\lambda_{cl}^2(T=0)}\left\{\frac{\pi}{2\alpha}-\frac{1}{\alpha\sqrt{1-\alpha^2}}\times\sin^{-1}(\sqrt{1-\alpha^2})\right\},\quad \alpha<1$$
$$\frac{1}{\lambda_{cl}^2(T=0)}\left\{\frac{\pi}{2\alpha}-\frac{1}{2\alpha\sqrt{\alpha^2-1}}\ln\left(\frac{\alpha+\sqrt{\alpha^2-1}}{a-\sqrt{\alpha^2-1}}\right)\right\},\quad \alpha>1. \tag{9}$$

In the weak scattering limit this expression reduces to the more familiar form,

$$\frac{1}{\lambda^2(0)}\approx\frac{1}{\lambda_{cl}^2(0)}\frac{1}{1+(\pi/4)\alpha}. \tag{10}$$

This expression can be written in terms of the zero-temperature coherence length ξ_0, and the mean free path l, using $\Delta=v_F/\pi\xi_0$ and $v_F=l/\tau$, where v_F is the Fermi velocity:

$$\frac{1}{\lambda^2(0)}\approx\frac{1}{\lambda_{cl}^2(0)}\frac{1}{1+(\pi^2/8)(\xi_0/l)}. \tag{11}$$

In Fig. 4 we plot $\nu\sigma_2(\nu)$ at various frequencies as a function of the scattering rate, $1/\tau$. Clearly, up to about 5 meV the deviations from the zero-frequency curve, Eq. (9), are small. Significant deviations begin to occur at higher frequencies ($\nu=10$ meV). Thus, one must be careful when using finite frequency data to infer information about the zero-frequency penetration depth.

IV. THE STRONG-COUPLING CASE

The results presented so far are based on BCS theory, where the interaction is modeled by a constant, structureless

in momentum and frequency (except for a cutoff). One of the merits of such an approach is that the results are universal, but the disadvantage is that inelastic scattering is not included and so strong-coupling effects in the superconducting state are not accounted for. Strong-coupling results first require a full numerical solution to the Eliashberg equations (1,2). Two parameters are needed to characterize a particular material, the electron-phonon spectral function $\alpha^2F(\omega)$, and the Coulomb repulsion, μ^*. The latter is often fitted to either T_c or the gap, while the former is extracted through an inversion procedure from tunneling data.[23] Often $\alpha^2F(\omega)$ has been found to be given roughly by a constant times the phonon frequency distribution, $F(\omega)$. Thus, for most purposes, the difference between $\alpha^2F(\omega)$ and $F(\omega)$ can be ignored and a single multiplicative parameter can be used to obtain $\alpha^2F(\omega)$ from $F(\omega)$ when tunneling data is not available. To be specific here, we will treat only the case of $Ba_{1-x}K_xBiO_3$. Its frequency distribution is known[24] and is similar to calculated[25] values of $\alpha^2F(\omega)$ as well as values determined from tunneling.[26] Based on these three spectra then if $Ba_{1-x}K_xBiO_3$ is an electron-phonon superconductor, the value of the electron mass renormalization $\lambda = 2\int d\omega\ \alpha^2F(\omega)/\omega$ needed to produce superconductivity with $T_c \approx 30$ K is $\lambda \approx 1$. Because of difficulties with the inversion of the tunneling data,[26] we will use a spectrum scaled from neutron-scattering results with $\lambda = 1$ as a representative intermediate coupling Eliashberg superconductor. In fact Sharifi *et al.* have argued, based on tunneling measurements, that $Ba_{1-x}K_xBiO_3$ is not an electron-phonon based superconductor.[27] In the next section we will also argue that $Ba_{1-x}K_xBiO_3$ cannot be an electron-phonon superconductor and that λ is more likely to be of order 0.2, a value much smaller than considered in the work previously quoted.[24–26]

In Fig. 5(a) we show results for the product of the frequency times the imaginary part of the conductivity, i.e., $\nu\sigma_2(\nu)$, as a function of ν for a strong-coupling superconductor with $\lambda = 1$ and $T_c = 29$ K as discussed above. The curves are plotted in the clean limit, i.e., $1/\tau = 0$. Scattering is still possible through inelastic scattering via the phonons, which are present at finite temperature. At low temperatures a very sharp Drude-like peak will be present in the normal-state conductivity. This manifests itself in the imaginary part of the conductivity as a sharp inverted Drude-like minimum near the origin,[28] as is visible in the lower left portion of Fig. 5(a). The solid curve is for $T/T_c = 0.99$ while the dotted curve, which is almost indistinguishable from the solid curve, is for the normal state at the same temperature. This curve extends down to zero at the origin (not shown) and has a width of order 1 meV. Also shown are results at $T/T_c = 0.5$ (dashed curve) and $T/T_c = 0.2$ (dot-dashed curve). These curves are very different from their counterparts in the previous section. The first thing to note is that sharp structure at $\nu = 2\Delta \approx 10.4$ meV is completely absent. In this case there is no BCS reference, as in this limit the corresponding result would be a constant at value unity (see Fig. 1). Recall that in the real part of the conductivity absorption begins beyond 2Δ not in an abrupt fashion as in the Mattis-Bardeen limit of the theory, but smoothly, roughly following the phonon density of states since the phonons conserve the energy and account for the momentum of the created electron-hole pair.[8,29] Since the absorption edge is not abrupt in $\sigma_1(\nu)$, we cannot expect

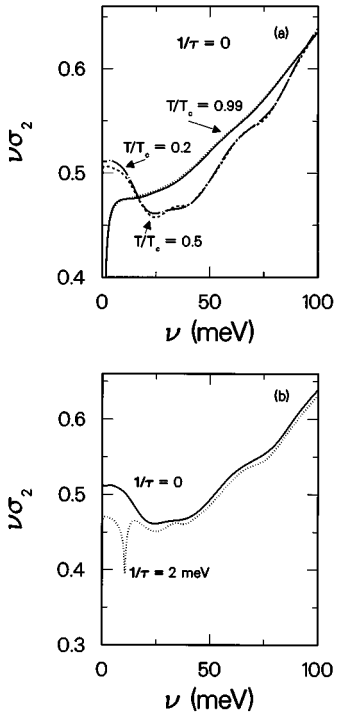

FIG. 5. $\nu\sigma_2(\nu)$ vs frequency as calculated using an electron-phonon spectrum with $\lambda = 1$ and $T_c = 29$ K as described in the text. In (a) we use $1/\tau = 0$ (clean limit) and plot the results for various temperatures, as indicated. The solid (dotted) curve is for the superconducting (normal) state at $T/T_c = 0.99$. Clearly there is very little difference throughout the frequency scale shown. Note the lack of a cusplike minimum at $\nu = 2\Delta_0 \approx 10.4$ meV. In (b) we focus on the low-temperature results ($T/T_c = 0.2$) and show the effect of a small amount of impurity scattering. The cusplike minimum at 2Δ is clearly present.

the corresponding sharp structure in the imaginary part $\nu\sigma_2(\nu)$; this is born out by our calculations shown in Fig. 5(a).

Another difference which is obvious upon inspection of Fig. 5(a) is that structure is present in the imaginary part of the conductivity over a frequency range representative of the phonon energies in the $\alpha^2F(\omega)$ spectrum. They occur here in much the same way as in the real part of the conductivity,[5,13] and leave open the possibility for the determination of $\alpha^2F(\omega)$ by infrared spectroscopy.

Finally another clear difference occurs in the zero-frequency limit, where, at low temperatures, the intercept is approximately 0.5, i.e., half of the London limit. This is due to phonon renormalization effects, which, for the most part amount to a $1+\lambda$ enhancement of the mass, as is obvious from Eq. (8).[30]

For nonzero impurity scattering two important things happen, as Fig. 5(b) shows. A cusplike minimum, conspicuous by its absence in the clean limit, is now present even with a small impurity scattering rate, $1/\tau = 2$ meV. Secondly the penetration depth, given by the inverse of the zero-frequency limit of the quantity plotted (see remark in the introduction), has increased with the addition of impurities, as discussed in the previous section in the BCS limit. The increase here is nonuniversal, i.e., it depends on the strength of the interac-

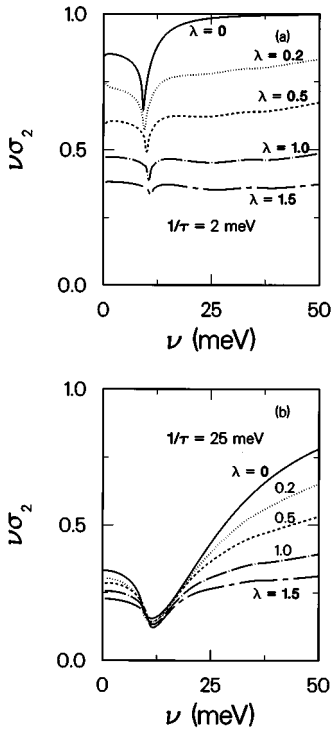

FIG. 6. $\nu\sigma_2(\nu)$ vs frequency for various coupling strengths, as indicated. The results are for low temperature $T/T_c=0.3$ and (a) relatively clean, $1/\tau=2$ meV, and (b) $1/\tau=25$ meV. The Coulomb repulsion μ^* has been adjusted to keep T_c fixed while the coupling strength has changed [simply by scaling the $\alpha^2F(\omega)$ spectrum]. Increased coupling strength suppresses $\nu\sigma_2(\nu)$ and broadens the minimum at 2Δ. Note that 2Δ increases slightly as the coupling strength is increased.

tion, and somewhat less sensitively on the form of the underlying electron-phonon spectral function.

To see the effect of coupling strength on the low-frequency imaginary part of the conductivity, the quantity $\nu\sigma_2(\nu)$ is plotted in Fig. 6 vs frequency with (a) $1/\tau=2$, and (b) $1/\tau=25$ meV. The curves plotted are for various coupling strengths as indicated, with the Coulomb repulsion μ^* adjusted in each case so that T_c remains 29 K. We have used a small Coulomb repulsion to model $Ba_{1-x}K_xBiO_3$ with $\lambda=1$ so that for small λ we use negative μ^*'s, thus representing some additional attractive mechanism by which the electrons bind. In Fig. 6(a) there is a clear lowering of the imaginary part of the conductivity with increasing coupling strength, while in Fig. 6(b) the value of $\nu\sigma_2(\nu)$ is drastically reduced even in the BCS limit ($\lambda=0$). In both cases the depth and sharpness of the minimum associated with 2Δ decreases as the coupling strength increases. The minimum also shifts slightly to higher frequency, as expected since the zero-temperature gap increases with increasing coupling strength. At higher frequencies phonon structure becomes more noticeable as coupling strength increases.

In Fig. 7 we show similar results to those given in Fig. 5 but now with an impurity scattering rate equal to 50 meV. Upon comparison with Fig. 5, it is clear that the entire curve for $\nu\sigma_2(\nu)$ at low temperatures ($T/T_c=0.2$) has been reduced systematically by the impurity scattering. Furthermore a gap minimum is clearly present, as Fig. 5(b) would suggest. Phonon structure is still seen at higher energies. Also, the value of the penetration depth has been reduced significantly in a fashion that roughly obeys Eq. (9). There are strong-coupling corrections[21] so that exact agreement is not expected.

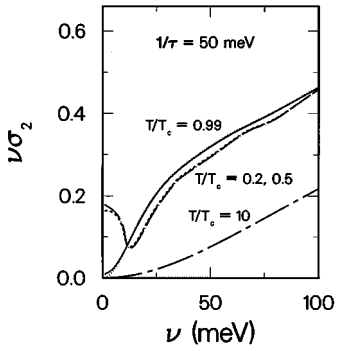

FIG. 7. $\nu\sigma_2(\nu)$ vs frequency for $1/\tau=50$ meV. The other parameters are the same as used in Fig. 5. The various curves are for different temperatures, $T/T_c=0.99$ (solid, superconducting; dotted, normal), $T/T_c=0.5$ (dashed), and $T/T_c=0.2$ (long-dashed). Both the first pair and the second pair of curves differ from one another only at very low frequency. Also shown is the normal-state result at $T/T_c=10$.

The higher temperature curves are also quite interesting and deserve some attention. The solid curve is for the superconducting case with $T/T_c=0.99$ and falls almost exactly on the dotted curve which is the normal-state result at the same temperature (differences are only apparent at very low frequency). In the normal state, the low-frequency part of the real and imaginary part of the conductivity can be fit to a Drude-like contribution, as first attempted by Dolgov, Moksimov, and Shulga[31] and taken up more microscopically and rigorously recently by two of us.[13] If both real and imaginary parts are fitted in a low-frequency expansion of the normal-state conductivity, we arrive at the result

$$\sigma_{\rm Drude}\equiv\frac{ne^2}{m}\frac{1}{1+\tilde{\lambda}}\frac{\tilde{\tau}}{1-i\nu\tilde{\tau}}, \tag{12}$$

with

$$\tilde{\tau}\equiv\frac{\langle[\tau^*(\omega)]^2/[1+\lambda^*(\omega)]\rangle}{\langle\tau^*(\omega)/[1+\lambda^*(\omega)]\rangle}, \tag{13}$$

and

$$1+\tilde{\lambda}\equiv\tilde{\tau}\Big/\left\langle\frac{\tau^*(\omega)}{1+\lambda^*(\omega)}\right\rangle, \tag{14}$$

with

$$1+\lambda^*(\omega)\equiv\frac{\partial\,\mathrm{Re}\tilde{\omega}(\omega)}{\partial\omega} \tag{15}$$

and

$$1/\tau^*(\omega)\equiv\frac{1/\tau+2\,\mathrm{Im}\tilde{\omega}(\omega)}{1+\lambda^*(\omega)}. \tag{16}$$

Note that $\langle Q(\omega)\rangle\equiv\int_0^\infty(\beta\,d\omega/2)\mathrm{sech}^2(\beta\omega/2)Q(\omega)$ and explicit closed expressions for both these last quantities are given in our previous paper.[13]

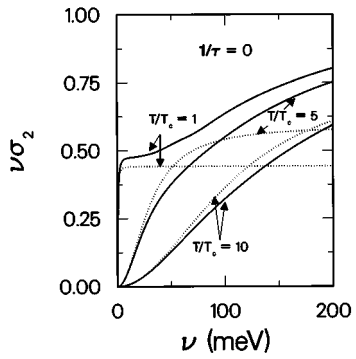

FIG. 8. $\nu\sigma_2(\nu)$ vs frequency for $1/\tau=0$ (clean limit) in the normal state, using the same parameters for the spectrum as in Fig. 5. The solid curves are results of complete Eliashberg calculations whereas the dotted curves are for the derived low-frequency Drude fits to the complete results. Curves are labeled by their reduced temperatures.

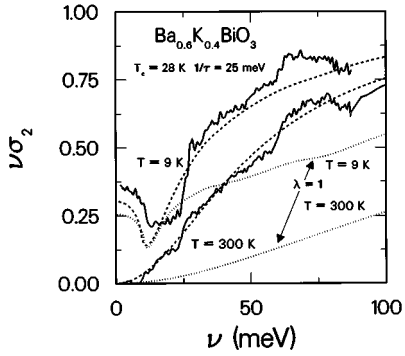

FIG. 9. The measured $\nu\sigma_2(\nu)$ vs frequency at $T=9$ K and at $T=300$ K (solid curves). Also shown are the theoretical fits, using the $\alpha^2F(\omega)$ described in the text, but with $\lambda=0.2$ (dashed curves). T_c is kept fixed to the experimental value with a negative μ^*. Finally, theoretical fits are also shown with $\lambda=1$ (dotted curves). The latter curves are clearly incompatible with the experimental results.

In Fig. 8 we compare our Drude fits (dotted curves) with the full electron-phonon results (solid curves) in the clean limit as a function of frequency for various temperatures in the normal state. At low temperature, i.e., $T/T_c=1$, the Drude fit at low frequency is very narrow, reflecting the fact that the electron-phonon scattering time becomes very long at low temperature. As the frequency increases the two curves begin to deviate very markedly. In units of ne^2/m, $\nu\sigma_2(\nu)$ as modeled by the Drude form Eq. (12) will saturate at high frequencies to a value of $1/(1+\tilde{\lambda})$, which is 0.43 for the chosen parameters. This saturation is seen very clearly in the plots. As the temperature is increased to $T/T_c=5$, the inelastic scattering increases significantly. The solid curve reflects this fact in that the low-frequency variation is on a much larger scale, of order 60 meV. Also, the Drude-like curve (dotted) fits the full numerical solution (solid curve) over a larger frequency range and saturates at a larger value of $1/(1+\tilde{\lambda})$, which has increased considerably with increasing temperature as described in our previous work.[13] Note that $\lim_{\nu\to\infty}\nu\sigma_2(\nu)=1$ in the full calculation (in units of ne^2/m). Thus, one could use $\nu\sigma_2(\nu)$ data to determine $\tilde{\lambda}$ and $\tilde{\tau}$ independently from the low-frequency fit and from the infinite frequency limit. Finally, the last set of curves is for $T/T_c=10$. The fit is very good at low frequency. The two curves cross just beyond the highest frequency shown, and large deviations occur there.

Returning to Fig. 7, the short-dashed-long-dashed curve is given for $T/T_c=10$ (290 K). The width of the imaginary part of the conductivity has increased drastically over its value for $T/T_c=1$. This increase is due entirely to the increased inelastic scattering at elevated temperatures. The total width, of course, is a combination of the inelastic and elastic contribution; this is clear from a comparison of the $T/T_c=1$ curves of Figs. 5 and 7. In Fig. 5, the width of the imaginary part of the conductivity is very narrow because it is only due to inelastic scattering, while in Fig. 7 it is almost entirely due to the elastic scattering provided by a $1/\tau=50$ meV impurity term. While one might think that a lower bound for this width is 50 meV, one must recall that the effective elastic-scattering rate is renormalized by the electron-phonon interaction. It is well known[30,32] that the electron-phonon interaction renormalizes $1/\tau$ by a factor $1/(1+\lambda)$, which is about 0.5 in our calculations. This is why the effective width in Fig. 7 appears to be smaller than 50 meV, and close to 25 meV.

V. THE SPECIFIC CASE OF $Ba_{1-x}K_xBiO_3$

Puchkov and co-workers[33,34] have obtained experimental results for the conductivity in samples of $Ba_{1-x}K_xBiO_3$ with varying x in the superconducting region of the phase diagram. Based on an analysis of the real part of the conductivity, the authors of Ref. 33 conclude, contrary to the conclusions of many other workers,[24–26] that this material cannot be a conventional electron-phonon superconductor with coupling constant value $\lambda\approx1$. This conclusion was reinforced by the more precise microscopic analysis provided by two of us.[13] Here, we extend our theoretical analysis to the imaginary part. In Fig. 9 we plot the quantity $\nu\sigma_2(\nu)$ as a function of frequency at two different temperatures, one in the superconducting state, and one in the normal state. The experimental spectra were obtained using a Kramers-Kronig analysis of the reflectivity spectra measured from 25 to 40 000 cm^{-1} as was reported elsewhere.[33] To improve the accuracy of the analysis, ellipsometric measurements were performed on the same crystal at frequencies from 10 000 to 50 000 cm^{-1}, and the high-frequency reflectivity approximation was chosen in such a way that the calculated high-frequency optical conductivity was in agreement with the direct ellipsometric results. Note that we have used the data at 1500 cm^{-1} (185 meV) to normalize the curves.

The most striking feature of the data in Fig. 9 is the well-defined minimum which occurs at approximately 12 meV. In light of the discussion thus far we view this result as unequivocal evidence of an s-wave order parameter in the $Ba_{1-x}K_xBiO_3$ system. Similar results for other dopant concentrations (and hence T_c's) are also obtained.[34] This conclusion is reinforced by complementary work by Jiang and Carbotte[35] wherein they investigate the behavior of the imaginary part of the conductivity for a superconductor with order parameter of d-wave symmetry. They find that no minimum occurs in $\nu\sigma_2(\nu)$ at 2Δ, in agreement with experi-

mental results on $YBaCu_3O_{7-x}$, which is generally believed to be a d-wave superconductor. This is what is expected since the real part of the conductivity does not have an abrupt onset at 2Δ, which we have argued accompanies the minimum in the imaginary part via a Kramers-Kronig transform.

Given the normalization of the experimental data discussed above, Fig. 2 makes it clear that a considerable amount of impurity scattering is required to achieve a qualitative agreement between theory and experiment. This observation is also consistent with the analysis of the real part of the conductivity, although in that instance a ''midinfrared contribution'' of unknown origin had to be subtracted from the data first. Then Fig. 6(b) shows that for λ of order unity, the large amount of inelastic scattering present at relatively high frequencies ($\approx$25–50 meV) will reduce the imaginary part of the conductivity, in disagreement with experiment. This disagreement will be even more significant at higher temperatures.

Theoretical curves are also plotted in Fig. 9 to more clearly illustrate these remarks. As a ''good'' representative fit we show results at the two temperatures using a reduced $\alpha^2F(\omega)$ for $Ba_{1-x}K_xBiO_3$ with $\lambda=0.2$ (dashed curves). We have used $1/\tau=25$ meV, a value which is consistent with that obtained experimentally from $\sigma_1(\nu)$[33,34] It is clear that the fit is quantitatively good. For comparison we also show the result using the full spectrum, i.e., with $\lambda=1$. It is obvious that such a fit is poor, and given our previous results, the reader can appreciate that no amount of parameter adjustment will yield good agreement with the data *at both temperatures*, while retaining λ of order unity. This general result is, of course, consistent with the conclusion inferred from the real part of the conductivity.[33,13] The analysis here, however, has the advantage that no data subtraction is required before the analysis. It has the disadvantage that a high-frequency scale is required to normalize the experimental data shown in Fig. 9.

VI. CONCLUSIONS

We have studied the frequency dependence of the imaginary part of the conductivity $\nu\sigma_2(\nu)$ for an s-wave superconductor. Universal BCS results are first established which show a sharp cusplike minimum in $\nu\sigma_2(\nu)$ at twice the gap value. This provides a very good method for determining the gap value and its temperature dependence. As the rate of elastic impurity scattering is increased, the gap structure becomes progressively smeared and shifts to higher frequency. This shift is completely uncorrelated with the gap value since the gap is independent of elastic impurity scattering in an isotropic s-wave superconductor. In the presence of impurity scattering strong-coupling effects modify the results by smearing the gap minimum, and renormalizing the low-frequency behavior through a renormalization $1/\tilde{\tau}\rightarrow 1/\tau/(1+\lambda)$.[36] In addition, structure is apparent in the phonon region. These are all quantitative changes. In contrast, qualitative changes occur in the clean limit, since then strong-coupling effects become the only source for electron scattering. In this case, there is no structure in $\nu\sigma_2(\nu)$ at twice the gap value because absorption across the gap can only proceed through a phonon-assisted mechanism needed to absorb the necessary momentum and energy. This means that the real part of the conductivity will become nonzero at a frequency of twice the gap plus the lowest phonon energy in the system. The phonon spectrum generally extends to zero frequency but the density of states for the phonons usually has an ω^2 dependence at low frequency. This leads to a rather gradual increase in absorption and no sharp structure in $\nu\sigma_2(\nu)$. When impurities are added, a qualitative change occurs because impurity-assisted absorption can now set in quite abruptly at 2Δ. This manifests itself in the imaginary part of the conductivity as a sharp cusplike minimum in $\nu\sigma_2(\nu)$.

Application of our calculations to the specific case of $Ba_{1-x}K_xBiO_3$ allows us to conclude, from a consideration of data on the imaginary part of the conductivity alone, that this system is an s-wave superconductor. On the other hand, further analysis suggests that the superconductivity is not phonon mediated as others have concluded. The data is consistent with an electron-phonon mass enhancement parameter of about $\lambda\approx 0.2$. Larger values of order unity suggested in the literature lead to much too large a scattering rate at room temperature.

In summary we believe that measurement of the imaginary part of the conductivity is a powerful alternative to determine both the symmetry and the value of the superconducting order parameter. Used with normal-state measurements, such a probe also allows us to infer the strength of the inelastic scattering present in a particular superconductor. In contrast, in a d-wave superconductor, there will be no gap minimum at 2Δ because in such a case there is an entire distribution of gaps, starting at value zero. The conductivity averages over these gaps, and this leads to smooth behavior in $\nu\sigma_2(\nu)$.

ACKNOWLEDGMENTS

This research was partially supported by the Natural Sciences and Engineering Research Council of Canada (NSERC) and by the Canadian Institute for Advanced Research (CIAR). We thank Dimitri Basov for helpful discussions.

[1] T. Timusk and D. B. Tanner, in *Physical Properties of High Temperature Superconductors I*, edited by D. M. Ginsberg (World Scientific, Singapore, 1989), p. 339; D. B. Tanner and T. Timusk, in *Physical Properties of High Temperature Superconductors III*, edited by D. M. Ginsberg (World Scientific, Singapore, 1989), p. 363.

[2] T. Holstein, Phys. Rev. **96**, 535 (1954); Ann. Phys. **29**, 410 (1964).

[3] D. Basov, R. Liang, D. A. Bonn, W. N. Hardy, B. Dabrowski, M. Quijada, D. B. Tanner, J. P. Rice, D. M. Ginsberg, and T. Timusk, Phys. Rev. Lett. **74**, 598 (1995).

[4] J. Bardeen L. N. Cooper, and J. R. Schrieffer, Phys. Rev. **108**, 1175 (1957).

[5] S. B. Nam, Phys. Rev. B **156**, 470 (1967); **156**, 487 (1967).

[6] W. Lee, D. Rainer, and W. Zimmermann, Physica C **159**, 535 (1989).

[7] N. E. Bickers, D. J. Scalapino, R. T. Collins, and Z. Schlesinger, Phys. Rev. B **42**, 67 (1990).

[8] R. Akis, J. P. Carbotte, and T. Timusk, Phys. Rev. B **43**, 12 804 (1991).
[9] F. Marsiglio, Phys. Rev. B **44**, 5373 (1991).
[10] E. J. Nicol, J. P. Carbotte, and T. Timusk, Phys. Rev. B **43**, 473 (1991).
[11] F. Marsiglio, R. Akis, and J. P. Carbotte, Phys. Rev. B **45**, 9865 (1992). In this reference we provide a derivation for the phonon self-energy at $q=0$, which is almost identical to the conductivity.
[12] F. Marsiglio, J. P. Carbotte, R. Akis, D. Achkir, and M. Poirier, Phys. Rev. B **50**, 7203 (1994).
[13] F. Marsiglio and J. P. Carbotte, Phys. Rev. B **52**, 16 192 (1995).
[14] G. M. Eliashberg, Zh. Eksp. Teor. Fiz. **38**, 966 (1960) [Sov. Phys. JETP **11**, 696 (1960)].
[15] F. Marsiglio, M. Schossmann, and J. P. Carbotte, Phys. Rev. B **37**, 4965 (1988).
[16] C. S. Owen and D. J. Scalapino, Physica (Amsterdam) **55**, 691 (1971).
[17] D. Rainer and G. Bergmann, J. Low Temp. Phys. **14**, 501 (1974).
[18] D. C. Mattis and J. Bardeen, Phys. Rev. **111**, 412 (1958).
[19] G. Rickayzen, *Theory of Superconductivity* (Interscience, New York, 1965).
[20] W. Zimmerman, E. H. Brandt, M. Bauer, E. Seider, and L. Genzel, Physica C **183**, 99 (1991).
[21] J. P. Carbotte, Rev. Mod. Phys. **62**, 1027 (1990).
[22] A. J. Berlinsky, C. Kallin, G. Rose, and A.-C. Shi, Phys. Rev. B **48**, 4074 (1993). There is a typographical error in their Eqs. (15) and (16).
[23] W. L. McMillan and J. M. Rowell, in *Superconductivity*, edited by R. D. Parks (Dekker, New York, 1969), Vol. 1, p. 561.
[24] C.-K. Loong, D. G. Hinks, W. Jin, M. H. Degani, D. L. Price, J. D. Jorgensen, B. Dabrowski, A. W. Mitchell, D. R. Richards, Y. Zheng, P. Vashishta, and R. K. Kalia, in *Electron-Phonon Interaction in Oxide Superconductors*, edited by R. Baquero (World Scientific, Singapore, 1991), p. 122; C.-K. Loong, P. Vashishta, R. K. Kalia, M. H. Degani, D. L. Price, J. D. Jorgensen, D. G. Hinks, B. Dabrowski, A. W. Mitchell, D. R. Richards, and Y. Zheng, Phys. Rev. Lett. **62**, 2628 (1989).
[25] K. Motizuki, M. Shirai, and N. Suzuki, in *Electron-Phonon Interaction in Oxide Superconductors* (Ref. 24), p. 176; M. Shirai, N. Suzuki, and K. Motizuki, J. Phys. Condens. Matter **1**, 2939 (1989); Solid State Commun. **73**, 633 (1990); J. Phys. Condens. Matter **2**, 3553 (1990).
[26] J. F. Zasadzinski, N. Tralshawala, Q. Huang, K. E. Gray, and D. G. Hinks, in *Electron-Phonon Interaction in Oxide Superconductors* (Ref. 24), p. 46; Q. Huang, J. F. Zasadzinski, N. Tralshawala, K. E. Gray, D. G. Hinks, J. L Tengand, and R. L. Greene, Nature (London) **347**, 369 (1990).
[27] F. Sharifi, A. Pargellis, R. C. Dynes, B. Miller, E. S. Hellman, J. Rosamilia, and E. H. Hartford, Jr., Phys. Rev. B **44**, 12 521 (1991).
[28] In the Drude model, $\sigma_2(\nu)=(\nu\tau)^2/1+(\nu\tau)^2$. This is what we mean when we use the term ''inverted Drude-like.''
[29] J. P. Carbotte, C. Jiang, D. Basov, and T. Timusk, Phys. Rev. B **51**, 11 798 (1995).
[30] G. Grimvall, *The Electron-Phonon Interaction in Metals* (North-Holland, New York, 1981).
[31] O. V. Dolgov, E. G. Maksimov, and S. V. Shulga, in *Electron-Phonon Interaction in Oxide Superconductors* (Ref. 24), p. 30.
[32] We have shown that the renormalization is actually $1/(1+\tilde{\lambda})$. However, $\lim_{T\to 0}\tilde{\lambda}(T)=\lambda$.
[33] A. V. Puchkov, T. Timusk, W. D. Mosley, and R. N. Shelton, Phys. Rev. B **50**, 4144 (1994).
[34] A. V. Puchkov, T. Timusk, M. A. Karlow, S. L. Cooper, D. D. Han, and D. A. Payne, Phys. Rev. B **52**, R9855 (1995).
[35] C. Jiang and J. P. Carbotte (unpublished).
[36] Note that the first-order effect of adding an additional inelastic-scattering process (electron-phonon coupling) to an elastic-scattering process (impurity scattering) is to *reduce* the overall scattering rate (at low temperatures). This occurs because the inelastic scattering reduces the spectral weight of the quasiparticle undergoing the scattering.